High performance Three Level ANPC Inverter with Thermal Balancing PWM Strategy for Grid Connected PV System

Hanen Messaoudi*, Afef Bennani-Benabdelghani**, Najiba Mrabet-Bellaaj***

*National Engineering School of Tunis, Université de Tunis El Manar, 1002 Tunis, Tunisia

** National Institute of Applied Sciences and Technologies, Université de Carthage, 1080 Tunis, Tunisia

***High Institute of Informatics, Université de Tunis El Manar, 1002 Tunis, Tunisia

(hanen.messaoudi6@gmail.com, afef.bennani@gmail.com, najiba.bellaaj@isi.rnu.tn)

Hanen Messaoudi, 1002 Tunis, Tel: +216 99895623, hanen.messaoudi6@gmail.com

Received: 19.08.2018 Accepted:21.10.2018

Abstract- This paper proposes a high performance grid connected Photovoltaic (PV) system based on a three-phase transformerless three level Active Neutral Point Clamped (3L-ANPC) inverter. The ANPC is one of the derived topologies from the Neutral Point Clamped (NPC) one, which is widely used for transformerless grid connected PV applications thanks to its inherent advantages such as: reduced voltage stress on its power switches, reduced output current THD, low $\frac{dv}{dt}$, high efficiency, and loss and heat balancing capability. The 3L ANPC topology has mainly been proposed to overcome the NPC major issue of unbalanced loss and temperature distribution among its power devices. Furthermore, the modulation strategy is a key issue for loss and temperature balancing inside the ANPC topology. In this paper, the 3L-ANPC PV inverter is controlled by a Thermal Balancing PWM (ThB-PWM) strategy. This strategy allows an efficient balance of the loss and temperature distribution inside the inverter and a reduced total dissipated losses when compared with the conventional PWM strategies. The effectiveness of the proposed grid connected PV system based on a 6 kW 3L-ANPC inverter controlled by the ThB-PWM strategy is proven through simulation tests performed on PSIM simulator.

Keywords- NPC inverter; ANPC inverter; ThB-PWM strategy; thermal balancing; transformerless PV inverter.

1. Introduction

The PV systems have become one of the most mature technologies and the fastest growing energy generating systems among various renewable energy resources [1-2]... Nearly 75% of installed PV systems in the world are grid connected [3]. Nowadays, the most efficient commercial PV panels available on the market are characterized by an efficiency of around 17% to 22.5% [4]. Hence, it's crucial to efficiently transform and consume the power produced by these panels. This can be guaranteed using highly reliable and efficient power electronics systems. The performance of the PV inverters is improved by employing three phase transformerless inverter topologies. Compared to their counterparts with transformers, the transformerless configurations have the advantages of smaller weight and size, lower cost, reduced installation complexity, in addition to the increase of the total efficiency of the whole PV system by nearly 2% [3-5]. However, the lack of the galvanic isolation causes the generation of ground leakage currents flowing between the grid and the PV system. Several transformerless power configurations have been proposed to reduce the leakage current for PV grid connected systems [6-10]. The multilevel converter topologies are the most mature and commonly used ones for such applications [11-13] due to their intrinsic advantages which are: 1) Reduced voltage stress on its power switches due to the voltage sharing between the series connected switches, 2) More than two output voltage levels leading to a perfect sinusoidal shape, and thus lower THD, 3) Reduced output filter size thanks to

lower $\frac{dv}{dt}$, 4) Lower switching losses, since lower voltage power switches are used leading to the improvement of the overall system efficiency [12,16-18]. Among various multilevel topologies, the three level Neutral Point Clamped (3L-NPC) was one of the mostly used topologies in three phase transformerless grid connected PV systems [6]. However, this topology has a major drawback of the unequal loss and heat distribution among its power devices [17] which limits the inverter switching frequency and the maximum achievable power and reduces sensitively its reliability [20-21]. To overcome this drawback, the 3L-ANPC topology was introduced in 2001 [22]. The ANPC is derived from the NPC topology where the clamping diodes of this later are replaced by active switches allowing additional degrees of freedom for its control. These degrees of freedom can be explored to propose original modulation strategies in order to evenly distribute the power losses and the junction temperatures among the inverter power devices. In fact, if an equal loss and heat distribution are realized inside the inverter, then the power range of the system will not be limited by one or two single switches and the operating area of each power switch will be optimally used. Therefore, the 3L-ANPC topology-based transformerless grid connected PV system can improve the efficiency and extend the service lifetime of the overall system [23].

This paper introduces a high performance three phase grid connected PV system based on a transformerless 3L-ANPC inverter controlled by a proposed ThB-PWM strategy. This strategy provides a better loss and heat distribution inside the inverter and a reduced total loss dissipation, compared with conventional PWM strategies [24]. The paper is organized as follows: in section 2, a brief state of the art of the most widely used three phase transformerless PV inverters is presented. Then, the proposed PV system configuration and its control architecture are detailed in section 3. Finally, in section 4 the performance evaluation of the investigated PV system is highlighted through the discussion of the obtained simulation results of a 6 kW grid connected PV system performed on PSIM simulator.

2. Three Phase Transformerless Grid Connected PV Inverters: State of the Art

The transformerless grid connected PV installations are characterized by lower cost and reduced weight and size compared with their counterparts with transformers. However, the absence of galvanic isolation will generate a highly switching Common Mode Voltage (CMV), resulting in a high ground leakage current flowing between the PV system and the grid as shown in Fig. 1. This current raises the current harmonics injected into the utility grid and the system losses, in addition to serious Electromagnetic Interference (EMI) issues. C_p is the parasitic capacitance formed between the conductive layers, polymers, glass, and frame of the PV system, V_{Cp} is the CMV, and I_{cm} is the leakage current. The value of C_p can achieve 1µF/kW depending on the PV cell technology.

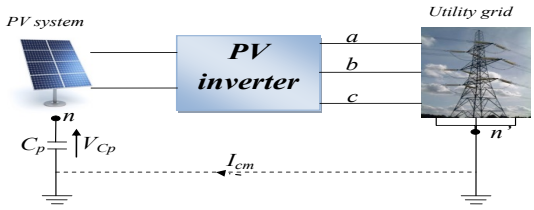

Fig.1. Leakage current in PV Grid connected system

The generated power by a transformerless grid connected PV system has to respect specific standard requirements. The most important norms concerning the connection of a PV system to the utility grid in a transformerless way are the grid current Total Harmonic Distortion (THD) which has been limited by the IEEE 1547 and the IEC 61727 standards to less than 5%, and the leakage current, that has been limited by the German standard VDE-0126-1-1 to less than 300 mA, else the disconnection from the grid is mandatory within 300ms.

The amplitude of the ground leakage current depends on the inverter topology and the modulation strategy [25]. Several topologies and control strategies have been proposed in order to reduce or eliminated the leakage current [26-30]…

2.1. Transformerless two level inverter

The conventional two level inverter is the simplest and the most commonly used topology for grid connected applications. However, the use of this topology without galvanic isolation leads to the generation of high amplitude leakage current flowing between the PV system and the grid caused by the high fluctuations of the CMV. Accordingly, the two level topology is not suitable for the transformerless grid connected configurations. Various topologies have been derived from the conventional two level one to reduce the leakage current by separating the PV system from the grid, such as the High Efficient and Reliable Inverter Concept (HERIC) where the AC side is disconnected during the zero switching state, the H5 and H7 topologies where the DC side is disconnected [8]… Furthermore, numerous modulation strategies permitting the reduction of the CMV fluctuations have been introduced, such as the Active Zero State PWM (AZSPWM) [28], the Near State PWM (NSPWM) [31], and the Remote State PWM (RSPWM) [32]. These modulation strategies are able to reduce the oscillation of the CMV and the leakage current. However, they generate overvoltage transients, high current ripples through the output filter, and high switching losses [33], which affect the whole system performances. Moreover, for high power applications, the PV system surface is huge, which increases its parasitic capacitance and hence, significantly increases the leakage current.

2.2. Transformerless NPC inverter

The NPC inverter is widely used for transformerless grid connected PV systems [6, 34-36]… It has proven to be of high efficiency and well suited for transformerless grid connected PV applications [6] since it's connected to the grid neutral and phases through the DC link neutral point and the output phase nodes, respectively. Thus, the problem of the high frequency commutations in the CMV is solved.

Consequently, there are no risks of high leakage current and Electromagnetic Interference (EMI).

Although, the major drawback of the NPC topology is the unbalanced power loss and junction temperature distribution inside the inverter [19]. Such a drawback can limit the inverter switching frequency and the power range of the whole system, and it can sensitively reduce its reliability and service lifetime. Therefore, the ANPC topology has been proposed [20] to overcome this issue. With its additional degrees of freedom, the ANPC inverter presents more controllability, which allows a better loss and junction temperature distribution among the inverter power devices.

2.3. *Transformerless ANPC inverter*

The three-phase 3L-ANPC topology is depicted in Fig. 2.

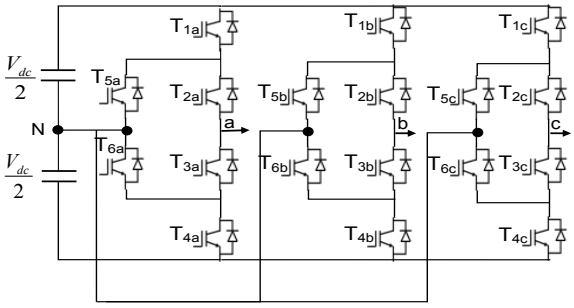

Fig. 2. Three-phase 3L-ANPC inverter topology

The additional degrees of freedom allow additional switching states and commutations [20] that can be exploited by the control strategy to balance the loss and the junction temperature distribution among the inverter power devices. The inverter can generate three output voltage levels: $-\frac{V_{dc}}{2}$, 0, $\frac{V_{dc}}{2}$ and it has six switching states summarized in Table 1, where I_{out} is the inverter output current.

According to Table 1, the 3L-ANPC inverter presents four possible zero state configurations designed, "z_1^u" and "z_2^u", if the output current flows through the upper path of the neutral point N and "z_1^l" and "z_2^l" if the output current flows through the lower one. The states "+" and "–" correspond to a direct connection of the output to the DC voltage source. It can be clearly observed from Table 1 that, even if there are more than two devices are turned off or on, only one diode and one active switch experience essential switching losses [12].

The selection of the commutation type may help to release the overheated devices and then balance the switching losses and the junction temperature distribution inside the inverter. The distribution of the conduction losses can be controlled by selecting the upper or the lower neutral path of the inverter. Thus, and as it has been proven in [21], the modulation strategy is the key factor that deeply influences the power loss and junction temperature distribution inside the 3L-ANPC inverter.

Table 1. The 3L-ANPC inverter switching states

Switching state	Output voltage	ON state device	Current direction	Most stressed devices
"+"	$\frac{V_{dc}}{2}$	$T_{1(a,b,c)}$, $T_{2(a,b,c)}$, $T_{6(a,b,c)}$	$I_{out} > 0$	$T_{1(a,b,c)}$, $T_{2(a,b,c)}$
			$I_{out} < 0$	$D_{1(a,b,c)}$, $D_{2(a,b,c)}$
"z_1^u"	0	$T_{2(a,b,c)}$, $T_{4(a,b,c)}$, $T_{5(a,b,c)}$	$I_{out} > 0$	$D_{5(a,b,c)}$, $T_{2(a,b,c)}$
			$I_{out} < 0$	$D_{2(a,b,c)}$, $T_{5(a,b,c)}$
"z_2^u"	0	$T_{2(a,b,c)}$, $T_{5(a,b,c)}$	$I_{out} > 0$	$D_{5(a,b,c)}$, $T_{2(a,b,c)}$
			$I_{out} < 0$	$D_{2(a,b,c)}$, $T_{5(a,b,c)}$
"z_1^l"	0	$T_{3(a,b,c)}$, $T_{6(a,b,c)}$	$I_{out} > 0$	$T_{6(a,b,c)}$, $D_{3(a,b,c)}$
			$I_{out} < 0$	$T_{3(a,b,c)}$, $D_{6(a,b,c)}$
"z_2^l"	0	$T_{1(a,b,c)}$, $T_{3(a,b,c)}$, $T_{6(a,b,c)}$	$I_{out} > 0$	$T_{6(a,b,c)}$, $D_{3(a,b,c)}$
			$I_{out} < 0$	$T_{3(a,b,c)}$, $D_{6(a,b,c)}$
"–"	$-\frac{V_{dc}}{2}$	$T_{3(a,b,c)}$, $T_{4(a,b,c)}$, $T_{5(a,b,c)}$	$I_{out} > 0$	$D_{4(a,b,c)}$, $D_{3(a,b,c)}$
			$I_{out} < 0$	$T_{3(a,b,c)}$, $T_{4(a,b,c)}$

3. Proposed 3L-ANPC Based Grid Connected PV System Configuration

The investigated three phase grid connected PV system is depicted in Fig. 3.

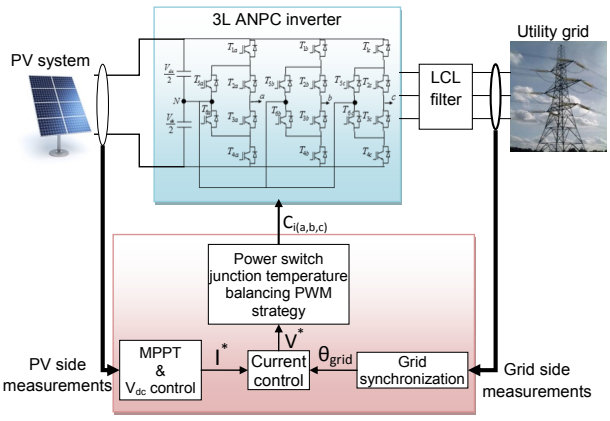

Fig. 3. Proposed 3L-ANPC based grid connected PV system

It compromises a PV power generation system connected to the utility grid through a three-phase transformerless 3L-ANPC inverter and a low pass LCL filter that reduces the current ripple, resulting in low harmonic distortion. To be connected to the utility grid, the inverter DC link voltage magnitude has to be greater than the peak value of the rms value of the AC line to line grid voltage.

Fig. 4 shows the proposed control of the considered PV system, which mainly compromises the proposed ThB-PWM

strategy that generates the three phase inverter power device gate signals $C_{i(a,b,c)}$, $i=1..6$.

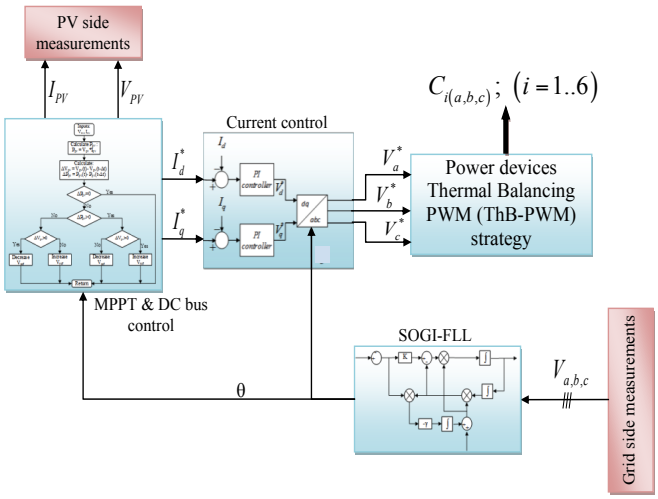

Fig. 4. Proposed control of the 3L-ANPC based grid connected PV system

The Maximum Power Point (MPP) is tracked using a suitable P&O based MPPT algorithm for a maximum power extraction from the PV system. The whole power produced by the PV system is injected into the grid. The P&O based MPPT algorithm inputs are the current I_{pv} and the voltage V_{pv} delivered by the PV system and it generates the DC bus reference voltage V_{dc}^{*} for the DC bus controller. This latter generates the reference current I^{*} for the current controller.

The simulation results of the MPPT of a 6.37 kW 3L-ANPC based grid connected PV system are depicted in Fig. 5. Where P_{max} is the maximum power point of the PV system and P_{pv} is the power absorbed by the grid.

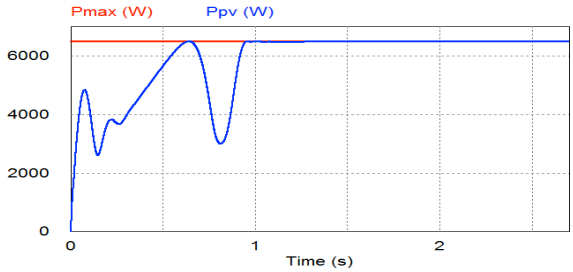

Fig. 5. Simulation result of the maximum power point of the proposed PV system

Fig. 6 shows the current I_{PV} and the voltage V_{PV} delivered by the PV system.

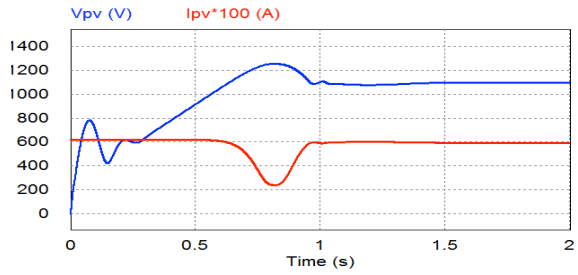

Fig. 6. Output current and voltage of the PV system

The Second Order Generalized Integrator - Frequency Locked Loop (SOGI-FLL) which is one of the most efficient grid synchronization techniques is employed. This technique permits not only the extraction of the grid voltage angle θ that will be used to synchronize the inverter output signals with the grid voltage, but it also permits a real time and accurate grid frequency adaptation [37]. Fig. 7 shows the waveform of the grid voltage angle θ and frequency ω generated by the SOGI-FLL.

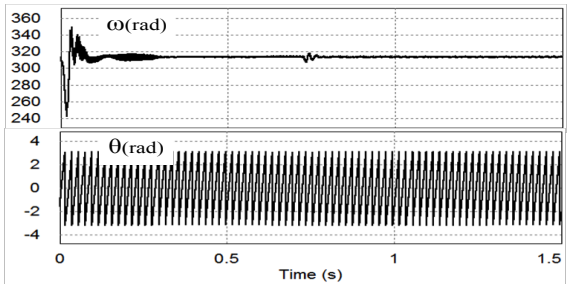

Fig. 7. Grid voltage angle and frequency generated by the SOGI-FLL

For the current control, the Voltage Oriented Control (VOC), which is one of the most commonly employed current control configuration for three phase grid connected PV inverter [37-38] is used in this paper. For a simplified control system design, VOC uses a rotational dq reference frame transformation oriented with the grid voltage vector in order to transform all the AC quantities to DC signals, so that it enables the use of the PI controller. It contains two main loops: an external voltage control loop that controls the DC link voltage V_{dc} via a PI controller to generate the reference currents in the dq frame, and an internal current loop, which delivers the reference voltages converter to the abc frame V_{a}^{*}, V_{b}^{*}, and V_{c}^{*} to the modulation strategy.

The output current I_a and the grid voltage V_{ga} of the phase "a" of the 3L-ANPC inverter and their harmonic spectrum are shown in Fig. 8.

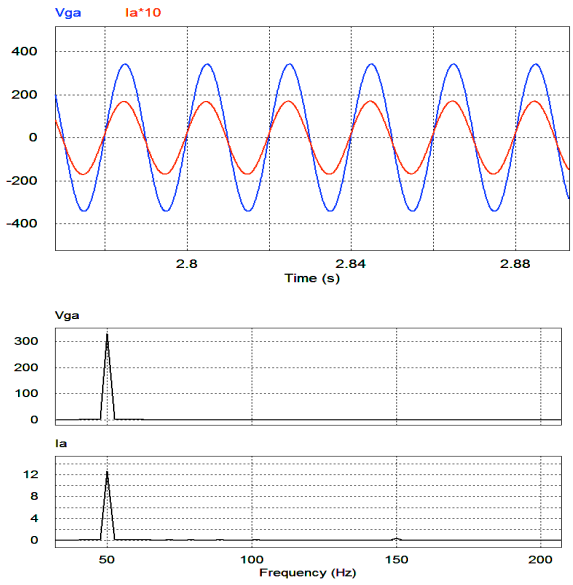

Fig. 8. Inverter output current and voltage and their harmonic spectrum of the phase a

According to Fig.8, the harmonic spectrum of the inverter output voltage and current shows the existence of a single high level harmonic at the switching frequency of the inverter, which reflects the perfect sinusoidal shape of the two signals.

An LCL filter is connected to the inverter output to reduces the current ripple; resulting in low harmonic distortion. The filter input voltage V_{a_in} and output voltage V_{a_out} are depicted in Fig 9.

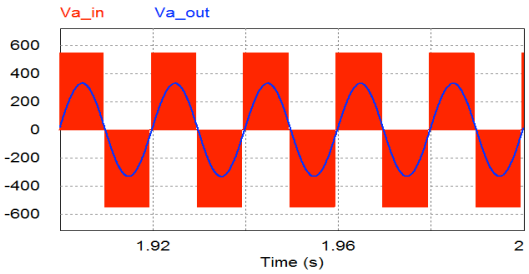

Fig. 9. LCL filter input and output voltages

The LCL filter input voltage is the inverter output voltage, which presents three different levels: $-\frac{V_{PV}}{2}$, 0, and $\frac{V_{PV}}{2}$. The inductance and capacitance values of the LCL filter are calculated based on the mathematical development and analysis proposed in [40].

4. Proposed Thermal Balancing PWM (ThB-PWM) Strategy

The Thermal Balancing PWM (ThB PWM) strategy has been firstly proposed in [21]. This proposed strategy is a combination of two classical PWM strategies named PWM_1 and PWM_2 taking benefits from their advantageous to evenly distribute the junction temperatures inside the inverter. The principle of the PWM_1 and the PWM_2 and their resulting gate signals C_{ia}, where $i = 1..6$ are depicted in Fig. 10 and Fig. 11 respectively.

These two modulation strategies are based on a comparison between a sinusoidal reference voltage V_{ref} switching at a low frequency (50 Hz) and two triangular carriers Tri_1 and Tri_2 switching at a high frequency (1 kHz).

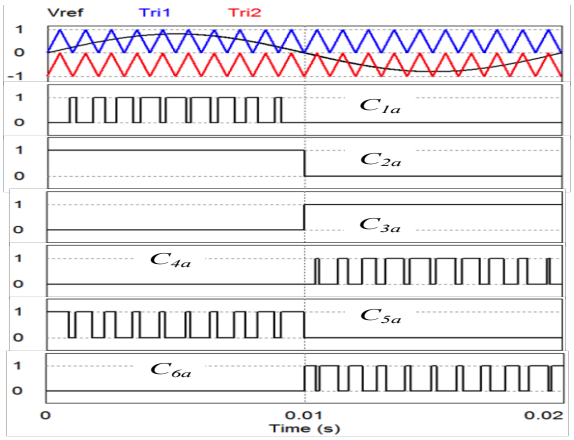

Fig. 10. Principle and resulting gate signals of the PWM_1

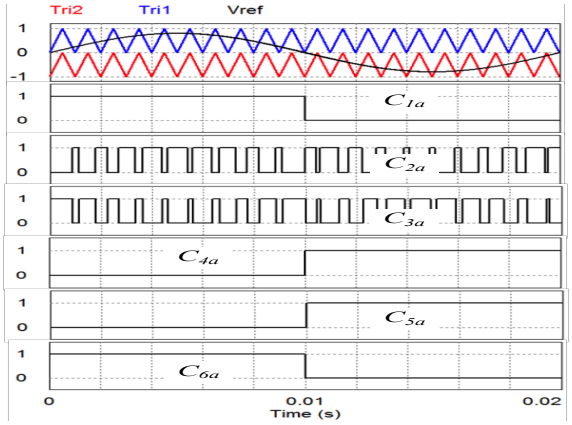

Fig. 11. Principle and resulting gate signals of the PWM_2

In contrary to all the conventional PWM strategies, the proposed strategy allows not only an even junction temperature distribution, but also it offers a significant reduction of the inverter total loss dissipation.

Fig. 12 presents the flowchart of the proposed ThB-PWM strategy.

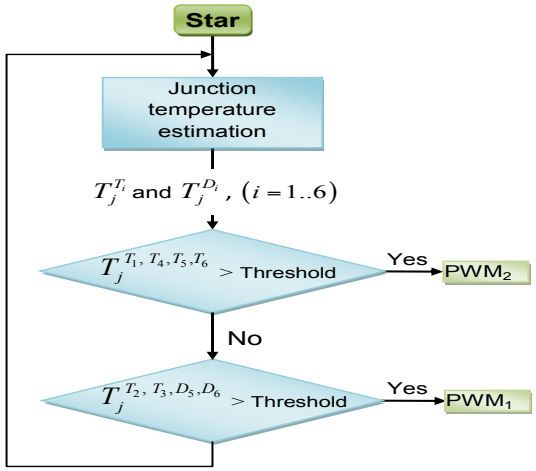

Fig. 12. Flowchart of the proposed ThB-PWM strategy

The gate signals generated by the proposed ThB-PWM strategy for the switching devices of the phase a are presented in Fig 13.

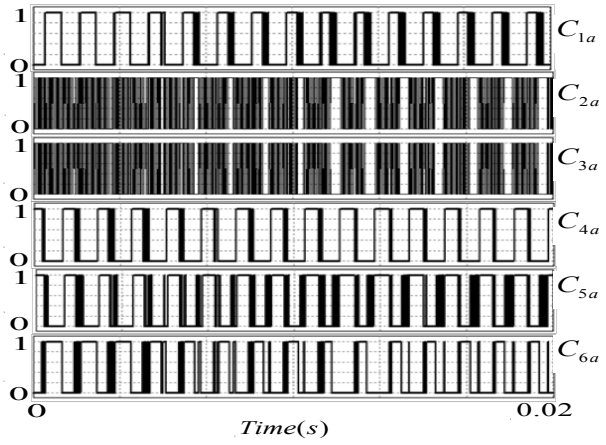

Fig. 13. Generated gate signals of the proposed ThB-PWM strategy

The algorithm of the proposed ThB-PWM strategy is based on two main functional units: the first unit is responsible for the real-time estimation of the power losses and the junction temperatures of the six converter active switches $T_j^{T_i}$ and their inverse diodes $T_j^{D_i}$, where $i = 1..6$.

The junction temperatures T_j of all the inverter power devices are estimated using an RC based Foster network as reported in [21]. T_j is a key factor describing the thermal behavior of the power semiconductors. The instantaneous junction temperature of the junction *j* is calculated by (1).

$$T_j(t) = P_{tot}(t) \times Z_{th(j-c)}(t) + T_{amb}(t) \quad (1)$$

It depends on the device's total dissipated power losses P_{tot}, which are also estimated using the loss models presented in [21], the ambient temperature T_{amb}, and the transient thermal impedance from the junction to the case $Z_{th(j-c)}$, which is available in the device datasheet.

The second unit is responsible for the generation of the gate signals, either by the PWM_1 or the PWM_2, according to the estimated junction temperature behavior in order to release the overheated device. Therefore, the junction temperatures of the most stressed power devices in the case of the two conventional PWM strategies are compared to a certain carefully chosen threshold. Thus, if one of these power devices junction temperature exceeds the threshold in the case of one of the PWM strategies (PWM_1 or PWM_2), the algorithm allows the other PWM strategy to generate the gate signals, and so on.

5. Simulation Results and Performance Evaluation

The PV system is made of a series connection of SUNPOWER E19/425 solar panels [41]. Fifteen solar panels are used in this work because for the grid connection applications the DC link magnitude has to be greater than the rms value of the AC line to line grid voltage. The electrical characteristics of a single solar panel are depicted in Table 2.

Table 2. Electrical characteristics of a a single SUNPOWER E19/425 solar panel [41]

Open circuit voltage (V_{oc})	85.6V
Maximum power point voltage (V_{MPP})	72.9V
Short circuit current (I_{sc})	6.18A
Maximum power point Current (I_{MPP})	5.83A
Maximum power (P_M)	425W

The simulation tests are performed on the PSIM simulator. The PSIM simulation diagram of the proposed system is shown in Fig. 16 and the simulation parameters are presented in Table 3.

Table 3. Simulation parameters

Parameter			Values
DC link capacitance			9 mF
Three phase grid parameters	Impedance	Inductance L_g	2 mH
		Resistance R_g	1 Ω
	Line to line voltage		400 V
	Frequency		50 Hz
LCL filter	Inductance L		4 mH
	Capacitance C		35 µF
Inverter switching frequency f_{sw}			10 kHz
PV system parasitic capacitance			300 nF

All the depicted simulation results are presented at the steady state. The performance evaluation of the grid connected PV system under investigation is performed through a comparative study made between a conventional two level inverter controlled by a traditional PWM strategy, a 3L-NPC inverter controlled by a DP PWM strategy [18], a 3L-ANPC inverter controlled by a high efficient and widely used PWM strategy [21], and a 3L-ANPC inverter controlled by the proposed ThB-PWM strategy. The compared inverter topologies are three phase transformerless ones and they are used to interface a 6.37 kW PV power generation system and the three phase utility grid. The comparison between these four inverter topologies is performed in terms of the injected power quality (grid current THD), the loss and junction temperature distribution inside the inverter, the CMV behavior, the leakage current, and the total efficiency η calculated by (2):

$$\eta = \frac{P_{out}}{P_{in}} = \frac{P_{out}}{P_{PV}} \quad (2)$$

Where P_{out} is the output power and P_{in} or P_{PV} is the input power delivered by the PV system.

In terms of grid current THD, the simulated proposed grid connected PV system presents a THD of about 27% in the case of the two level inverter. This THD value is very high and exceeds the limit fixed by the standards. Whereas, the current THD is reduced to about 4.7% when using the 3L-NPC inverter, which is quite below the limit, fixed by the IEEE and the IEC standards. In the case of the 3L-ANPC inverter controlled by the conventional PWM strategy, the grid current THD is about 9%. This value is significantly reduced compared with the two level inverter but it's higher than the 3L-NPC case and it exceeds the fixed limit. Finally, the THD in the case of the 3L-ANPC inverter controlled by the proposed ThB-PWM strategy is about 2.7%, which is well below the fixed limit and is very well improved compared to the previously mentioned topologies.

The simulation results shown in Fig 14 present the CMVs and the leakage currents for the four inverters.

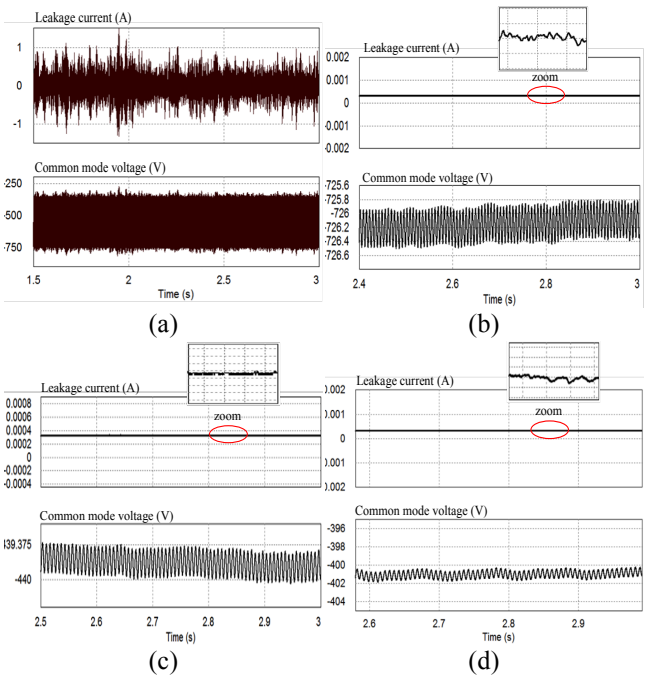

Fig. 14. CMV and leakage current in the case of the two level inverter (a), the 3L-NPC inverter (b), the 3L-ANPC inverter controlled by the conventional PWM strategy (c), and the 3L-ANPC inverter controlled by the proposed ThB-PWM strategy (d)

The CMV shown in Fig. 14.a corresponds to the two level inverter case. It's highly fluctuating causing a high leakage current that achieves 1.16 A. This value is significantly exceeding the limit fixed by the German standard. In the case of the 3L-NPC inverter, however, and according to Fig. 14.b, the CMV is nearly constant and its oscillations are significantly reduced compared to the previous case of the two level inverter. Thus, the leakage current is reduced to 0.33 mA, which is well below the fixed limit. According to Fig. 14.c, the oscillations of the CMV in the case of the 3L-ANPC inverter controlled by the conventional PWM strategy are significantly reduced compared with the two level inverter but not well improved compared to the case of the 3L-NPC inverter, and the leakage current is about 0.33 mA. For the 3L-ANPC inverter controlled by the proposed ThB-PWM strategy, the CMV shown in Fig. 14.d is nearly constant with more reduced fluctuations. Thus the leakage current is further reduced to about 0.27 mA. Summarily, with the 3L-NPC and the 3L-ANPC topologies, a small leakage current is generated, and this current is under the limit fixed by the German standards. Moreover, it also can be clearly observed that the use of the proposed ThB-PWM strategy to control the 3L-ANPC inverter can further reduce the leakage current.

The junction temperature distribution inside the inverter is a key criterion since it deeply affects its performances and the delivered power quality. The simulation results of the junction temperature distribution inside a single leg of each one of the considered inverters are presented in Fig 15.

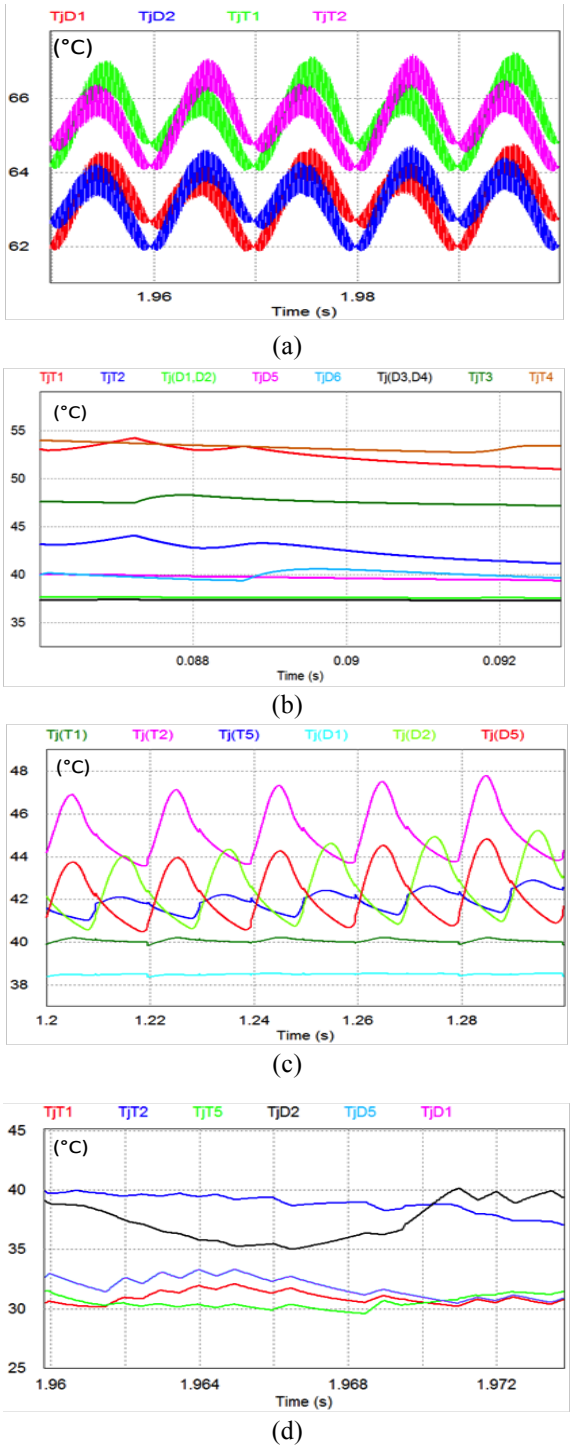

Fig. 15. Junction temperature distribution inside the two level inverter (a), the 3L-NPC inverter (b), the 3L-ANPC inverter controlled by the conventional PWM strategy (c), and the 3L-ANPC inverter controlled by the proposed ThB-PWM strategy (d)

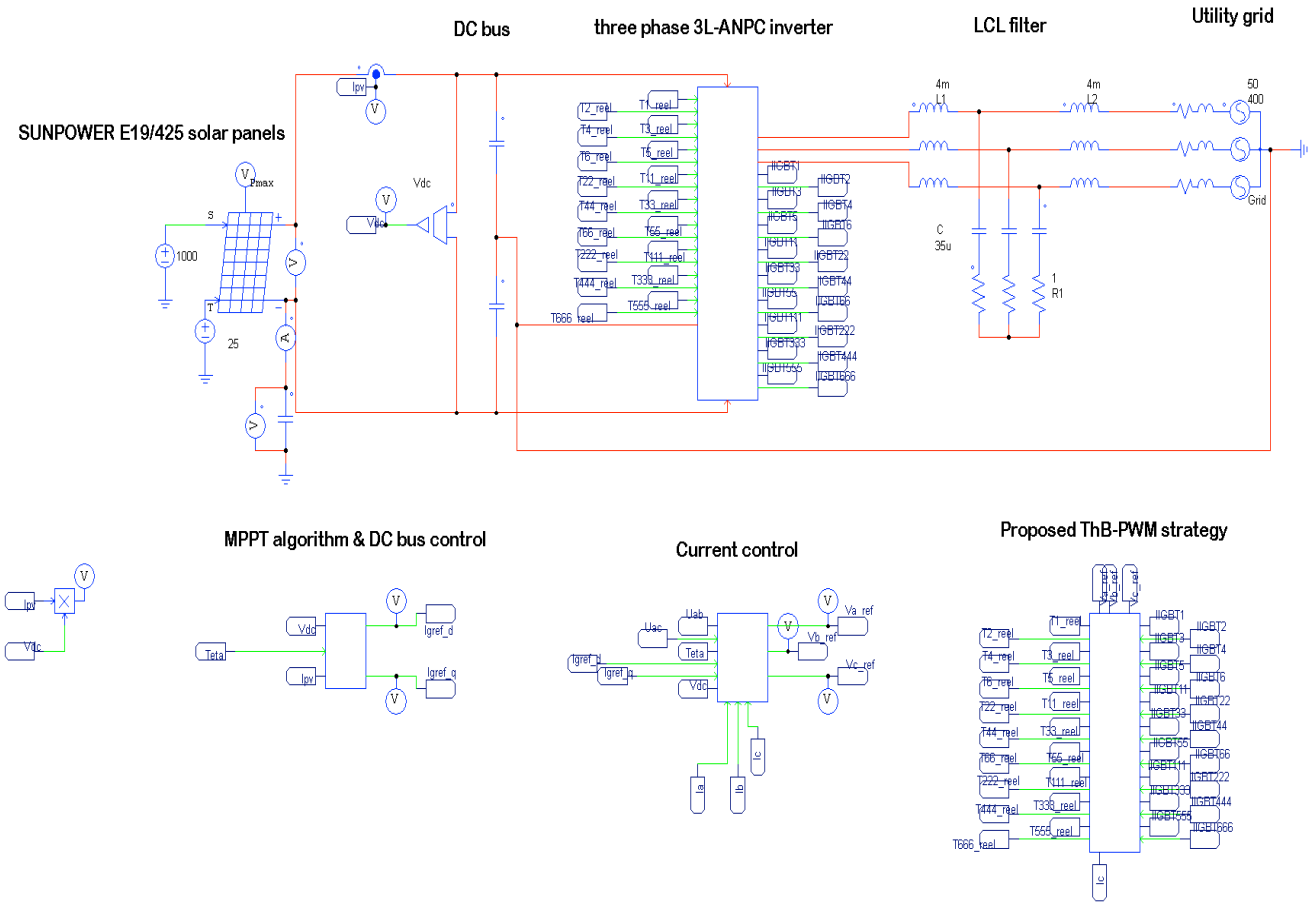

Fig. 16. PSIM simulation diagram of the proposed system

T_jT_1, T_jT_2, T_jD_1, and T_jD_2 shown in Fig. 15.a are respectively the junction temperature distribution among a single leg of the two level inverter power devices, which are two IGBTs: T_1 and T_2 and their inverse diodes: D_1 and D_2. Fig. 15.b presents the junction temperature distribution among a single leg of the 3L-NPC inverter power devices. The junction temperatures of the four IGBTs T_1, T_2, T_3, and T_4 are T_jT_1, T_jT_2, T_jT_3, and T_jT_4, respectively. Those of the IGBTs inverse diodes D_1, D_2, D_3, and D_4 are T_jD_1, T_jD_2, T_jD_3, and T_jD_4, respectively, and for the two clamping diodes D_5 and D_6 are T_jD_5 and T_jD_6, respectively. The junction temperatures of the 3L-ANPC inverter power devices are T_jT_i and T_jD_i, (i=1..6) corresponding to the six IGBTs T_i and their inverse diodes D_i, T_jT_5, (i=1..6), respectively. As the 3L-ANPC inverter is symmetric; the power devices T_1, T_2, T_5, D_1, D_2, D_5 have the same junction temperatures as T_4, T_3, T_6, D_4, D_3, D_6, respectively.

As shown in Fig. 15.a, the gap between the highest and the lowest temperature inside the two level inverter is about 7 °C, whereas inside the 3L-NPC inverter, and according to Fig. 15.b, this gap achieves 17°C, which is a high value highlighting the major drawback of the 3L-NPC inverter of the equal loss and junction temperature distribution among its power devices. In the case of the 3L-ANPC inverter controlled by the conventional PWM strategy shown in Fig. 15.c, this gap is reduced to about 8.9 °C due to the control strategy that allows an even loss and junction temperature distribution inside the inverter compared with the 3L-NPC case. The proposed ThB-PWM strategy allows a better loss and junction temperature distribution inside the 3L-ANPC inverter according to Fig. 15.d that shows that the gap between the highest and the lowest temperature is reduced to about 6 °C. Furthermore, the proposed ThB-PWM strategy permits a significant reduction of the maximum junction temperature to less than 40 °C, obviously the reduction of the total loss dissipation inside the inverter.

The efficiency is calculated by (2) for each inverter topology. For the conventional 2L inverter, the efficiency is about 94%. However, it achieves 98% for the 3L-NPC inverter, 98.5% for the 3L-ANPC inverter controlled by the conventional PWM strategy, and 99.8% in the case of the 3L-ANPC inverter controlled by the ThB-PWM strategy. These results can further prove the effectiveness and the high performances of the proposed transformerless grid connected PV system based on the 3L-ANPC inverter controlled by the ThB-PWM strategy.

The performance of the proposed system in terms of grid current THD, efficiency, leakage current, and junction temperature distribution among the inverter power devices is analyzed and compared with those of a traditional two level inverter, a 3L-NPC inverter, and a 3L-ANPC inverter controlled by a high efficient conventional PWM strategy. The simulation results are summarized in Table 4.

Table 4. Comparative summary of the performances of the four inverters topologies

PV inverter	Two level	3L-NPC	3L-ANPC + conventional PWM strategy	Proposed topology
Grid current THD	27%	4.7%	9%	2.7%
CMV fluctuations	very high	low	low	very low
Leakage current	1.16 A	0.33 mA	Am0.33	0.27 mA
Efficiency	94%	98%	98.5%	99.8%
Equal T_j distribution	high	very low	high	very high
Total dissipated losses	very high	very high	low	very low

6. Conclusion

A high efficiency grid connected PV system based on a transformerless 3L-ANPC inverter controlled by a thermal balancing PWM strategy is proposed in this paper. Besides, a brief review of the most widely used transformerless inverter topologies for grid connected PV applications is presented. The 3L-ANPV topology is an excellent candidate for such an application, with improved efficiency and injected power quality and reduced leakage current. The ThB-PWM strategy allows an even loss and junction temperature distribution among the inverter power devices, which improves the whole system performance.

The simulation results prove that the proposed PV system based on the 3L-ANPC inverter controlled by the ThB-PWM strategy presents the best performances since it provides high power quality with a reduced THD, a reduced leakage current flowing between the PV system and the grid, and a high efficiency achieving 99.8%. Furthermore, the considered 3L-ANPC controlled by the proposed ThB-PWM strategy provides the best junction temperature distribution among its power devices and a significant reduction of the total loss dissipation.

References

[1] D. Barater, C. Concari, G. Buticchi, E. Gurpinar, D. De, A. Castellazzi, "*Performance Evaluation of a Three-Level ANPC Photovoltaic Grid-Connected Inverter With 650-V SiC Devices and Optimized PWM* ", *IEEE Trans. Ind. Appl.*, vol. 52, n° 3, pp. 2475–2485, May 2016.

[2] S. Sezen, A. Aktas, M. Ucar, E. Ozdemir, "*A three-phase three-level NPC inverter based grid-connected photovoltaic system with active power filtering* ", in *2014 16th International Power Electronics and Motion Control Conference and Exposition*, pp. 1331–1335, 2014.

[3] D. C. Martins, "*Analysis of a Three-Phase Grid-Connected PV Power System Using a Modified Dual-Stage Inverter*", *International Scholarly Research Notices*, 2013.

[4] "2018 Most Efficient Solar Panels on the Market | EnergySage", *Solar News*, 13 March 2018.

[5] A. Bilal, M. Wilmar, K. Jorma. "*Performance analysis of a transformerless solar inverter with modified PWM*". In IEEE 6th International Conference on Renewable Energy Research and Applications (ICRERA). pp. 1024-1029, 2017.

[6] K. C. Oliveira, M. C. Cavalcanti, J. L. Afonso, A. M. Farias, F. A. S. Neves, "*Transformerless photovoltaic systems using neutral point clamped multilevel inverters"*, in the IEEE International Symposium on Industrial Electronics, pp. 1131–1136, 2010.

[7] R. Gonzalez, J. Lopez, P. Sanchis, L. Marroyo, "*Transformerless Inverter for Single-Phase Photovoltaic Systems"*, IEEE Trans. Power Electron. vol. 22, n° 2, pp. 693–697, March 2007.

[8] M. C. Poliseno, R. A. Mastromauro, M. Liserre, "*Transformer-less photovoltaic (PV) inverters: A critical comparison*", in the IEEE Energy Conversion Congress and Exposition (ECCE), pp. 3438–3445, 2012.

[9] S. B. Kjaer, J. K. Pedersen, F. Blaabjerg, "*A review of single-phase grid-connected inverters for photovoltaic modules*", IEEE Trans. Ind. Appl., vol. 41, n° 5, pp. 1292–1306, Sept. 2005.

[10] T. Kerekes, D. Séra, L. Máthé, "*Three-phase Photovoltaic Systems: Structures, Topologies, and Control*", Electr. Power Compon. Syst., vol. 43, n° 12, p. 1364–1375, Juill. 2015.

[11] M. Calais, V. G. Agelidis, "*Multilevel converters for single-phase grid connected photovoltaic systems-an overview*", in the IEEE International Symposium on Industrial Electronics. Proceedings (ISIE '98), vol. 1, p. 224–229, 1998.

[12] L. G. Franquelo, J. Rodriguez, J. I. Leon, S. Kouro, R. Portillo, M. A. M. Prats, "*The age of multilevel converters arrives*", IEEE Ind. Electron. Mag., vol. 2, n° 2, pp. 28–39, June 2008.

[13] S. B. Bahir, A. R. Beig, M. Poshtan, "An improved space vector PWM for grid connected MMC ", in 2017 IEEE 6th International Conference on Renewable Energy Research and Applications (ICRERA), pp. 556-561, 2017.

[14] W. Li, Y. Gu, H. Luo, W. Cui, X. He, C. Xia, "*Topology Review and Derivation Methodology of Single-Phase Transformerless Photovoltaic Inverters for Leakage Current Suppression*", IEEE Trans. Ind. Electron., vol. 62, n° 7, pp. 4537–4551, July. 2015.

[15] H. D. Paulino, P. J. M. Menegáz, D. S. L. Simonetti, "*A review of the main inverter topologies applied on the integration of renewable energy resources to the grid*", in XI Brazilian Power Electronics Conference, pp. 963–969, 2011.

[16] V. Pires, J. F. Martins, D. Foito, C. Hão, "*A Grid Connected Photovoltaic System with a Multilevel Inverter and a Le-Blanc Transformer*", International Journal of Renewable Energy Research (IJRER), vol. 2, n° 1, pp. 84-91, March 2012.

[17] H. A. B. Siddique, A. R. Lakshminarasimhan, C. I. Odeh, R. W. De Doncker, "Comparison of modular multilevel and neutral-point-clamped converters for medium-voltage grid-connected applications ", in 2016 IEEE International Conference on Renewable Energy Research and Applications (ICRERA), Birmingham, United Kingdom, pp. 297-304, 2016.

[18] L. E. M. Calaca, E. G. A. Jesus, J. Dionisio Barros, « Multilevel converter system for photovoltaic panels », in 2016 IEEE International Conference on Renewable Energy Research and Applications (ICRERA), Birmingham, United Kingdom, pp. 913-918, 2016.

[19] T. Bruckner, S. Bernet, H. Guldner, "*The active NPC converter and its loss-balancing control*", IEEE Trans. Ind. Electron., vol. 52, n° 3, pp. 855-868, June 2005.

[20] K. Ma, F. Blaabjerg, "*Loss and thermal redistributed modulation methods for three-level neutral-point-clamped wind power inverter undergoing Low Voltage Ride Through*", in the IEEE International Symposium on Industrial Electronics, pp. 1880-1887, 2012.

[21] H. Messaoudi, A. B. B. Abdelghani, N. M. Bellaaj, M. Orabi, "*Thermal performance-based comparative study of PWM strategies for three-level ANPC converter*", in the 7th International Renewable Energy Congress (IREC), pp. 1-6, 2016.

[22] E. Hauk, R. Álvarez, J. Weber, S. Bernet, D. Andler, and J. Rodríguez, "*New Junction Temperature Balancing Method for a Three Level Active NPC Converter*", *EPE J.*, vol. 22, n° 2, p. 6-12, June 2012.

[23] L. Ma, T. Kerekes, R. Teodorescu, X. Jin, D. Floricau, M. Liserre, "*The high efficiency transformer-less PV inverter topologies derived from NPC topology*", in the 13th European Conference on Power Electronics and Applications, pp. 1-10, 2009.

[24] H. Messaoudi, A. B. B. Abdelghani, N. M. Bellaaj, M. Orabi, "*Reconfigurable ANPC converter PWM strategy for an improved junction temperature distribution*", in the International Conference on Recent Advances in Electrical Systems, Hammamet, Tunisia, pp. 214-219, *2016*.

[25] R. Rahimi, B. Farhangi, S. Farhangi, "*New topology to reduce leakage current in three-phase transformerless grid-connected photovoltaic inverters*", in the 7th Power Electronics and Drive Systems Technologies Conference (PEDSTC), pp. 421-426, 2016.

[26] S. A. Khan, Y. Guo, J. Zhu, "*A high efficiency transformerless PV grid-connected inverter with leakage current suppression*", in the 9th International Conference on Electrical and Computer Engineering (ICECE), pp. 190-193, 2016.

[27] F. T. K. Suan, N. A. Rahim, H. W. Ping, "*An improved three-phase transformerless photovoltaic inverter with reduced leakage currents*", in the *3rd IET International Conference on Clean Energy and Technology (CEAT)*, pp. 1-4, 2014.

[28] C. C. Hou, C. C. Shih, P. T. Cheng, A. M. Hava, "*Common-Mode Voltage Reduction Pulsewidth Modulation Techniques for Three-Phase Grid-Connected Converters*", IEEE Trans. Power Electron., vol. 28, n° 4, pp. 1971-1979, 2013.

[29] M. C. Cavalcanti, A. M. Farias, K. C. Oliveira, F. A. S. Neves, J. L. Afonso, "*Eliminating Leakage Currents in Neutral Point Clamped Inverters for Photovoltaic Systems*", IEEE Trans. Ind. Electron., vol. 59, n° 1, pp. 435-443, 2012.

[30] T. Salmi, M. Bouzguenda, A. Gastli, A. Masmoudi, "*A Novel Transformerless Inverter Topology Without Zero-Crossing Distortion*", International Journal of Renewable Energy Research (IJRER), vol. 2, n° 1, pp. 140-146, 2012.

[31] E. Un, A. M. Hava, "*A Near-State PWM Method With Reduced Switching Losses and Reduced Common-Mode Voltage for Three-Phase Voltage Source Inverters*", IEEE Trans. Ind. Appl., vol. 45, n° 2, pp. 782-793, 2009.

[32] M. C. Cavalcanti, K. C. de Oliveira, A. M. de Farias, F. A. S. Neves, G. M. S. Azevedo, F. C. Camboim, "*Modulation Techniques to Eliminate Leakage Currents in Transformerless Three-Phase Photovoltaic Systems*", IEEE Trans. Ind. Electron., vol. 57, n° 4, pp. 1360-1368, 2010.

[33] Y. Jiao, F. C. Lee, "*New Modulation Scheme for Three-Level Active Neutral-Point-Clamped Converter With Loss and Stress Reduction*", IEEE Trans. Ind. Electron., vol. 62, n° 9, pp. 5468-5479, 2015.

[34] T. Kerekes, R. Teodorescu, M. Liserre, C. Klumpner, M. Sumner, "*Evaluation of Three-Phase Transformerless Photovoltaic Inverter Topologies*", IEEE Trans. Power Electron., vol. 24, n° 9, pp. 2202-2211, 2009.

[35] S. Busquets-Monge, J. Rocabert, P. Rodriguez, S. Alepuz, J. Bordonau, "*Multilevel Diode-Clamped Converter for Photovoltaic Generators With Independent Voltage Control of Each Solar Array*", IEEE Trans. Ind. Electron., vol. 55, n° 7, pp. 2713-2723, 2008.

[36] L. Ma, X. Jin, T. Kerekes, M. Liserre, R. Teodorescu, P. Rodriguez, "*The PWM strategies of grid-connected distributed generation active NPC inverters*", in the IEEE Energy Conversion Congress and Exposition, pp. 920-927, 2009.

[37] P. Rodríguez, A. Luna, R. S. Muñoz-Aguilar, I. Etxeberria-Otadui, R. Teodorescu, F. Blaabjerg, "*A Stationary Reference Frame Grid Synchronization System for Three-Phase Grid-Connected Power*

Converters Under Adverse Grid Conditions", IEEE Trans. Power Electron., vol. 27, n° 1, pp. 99-112, 2012.

[38] M. Malinowski, M. P. Kazmierkowski, A. M. Trzynadlowski, "*A comparative study of control techniques for PWM rectifiers in AC adjustable speed drives*", IEEE Trans. Power Electron., vol. 18, no 6, pp. 1390-1396, 2003.

[39] S. Cunningham, A. Nasiri, " Control and implementation of back to back grid converters utilizing IEEE 519 ", in 2017 IEEE 6th International Conference on Renewable Energy Research and Applications (ICRERA), San Diego, CA, pp. 345-347, 2017.

[40] M. Ben Said-Romdhane, M.W. Naouar, I. Slama-Belkhodja, E. Monmasson, "*An Improved LCL Filter Design in Order to Ensure Stability without Damping and Despite Large Grid Impedance Variations*", Energies, vol.10, pp.363-382, 2017.

[41] SunPower, *" SunPower Homepage ",* Available online on: https://us.sunpower.com/, [Consulted on: 10 October 2017].